Multiband Fermi surface in math xmlns="http://www.w3.org/1998/Math/MathML">mrow>mn>1/mn>mi>T/mi>mtext>−/mtext>msub>mi>VSe/mi>mn>2/mn>/msub>/mrow>/math> and its implication for the charge density wave phase

Turgut Yilmaz, Elio Vescovo, and Boris Sinkovic

Phys. Rev. B **107**, 165109 — Published 6 April 2023

DOI: 10.1103/PhysRevB.107.165109

Multi band Fermi surface in 1T-VSe_2 and its implication for charge density wave phase

Turgut Yilmaz and Elio Vescovo
*National Synchrotron Light Source II, Brookhaven National Lab, Upton, New York 11973, USA**

Boris Sinkovic
Department of Physics, University of Connecticut, Storrs, Connecticut 06269, USA
(Dated: March 29, 2023)

Angle resolved photoemission spectroscopy experiments reveal a surprisingly richer surface electronic structure in 1T-VSe_2 then previously predicted or probed. Earlier claims supporting a charge density wave phase in this material are re-examined in terms of these new findings and found to be untenable. The Fermi surface is found to be gapless, while band warping effects, currently attributed to 3D lattice distortion, result from the simultaneous dispersion of the closely laying multiple bands. Based on these new findings a charge density wave scenario in 1T-VSe_2 is unlikely. On the other side, the presence of multiple states crossing the Fermi level should constitute relevant constraints for any viable microscopic model of the structural phase transition of VSe_2.

I. INTRODUCTION

Layered transition metal dichalcogenides (TMDCs) host various electronic, structural, and transport phenomena making them most promising candidates for applications in electronic devices [1, 2]. Among the many novel states, the charge density wave (CDW) phase in these compounds is particularly under scrutiny as it often neighbors superconductivity domes in phase diagrams [3, 4]. In terms of electronic structure, the CDW phase is usually linked to Fermi surface nesting with associated gaps located at a specific portions of the Fermi surface connected by the CDW wave vectors [5–7]. In response to this electronic instability, atoms move from their original positions forming a superstructure that can be visualized through a scanning tunneling electron microscopy (STM) experiment [8–10].

Of all TMDCs, 1T-VSe_2 is a special example due to its long wavelength 3D-CDW phase in the bulk. It undergoes an incommensurate CDW with $4a \times 4a \times 3.18c$ periodic lattice distortion around $T^* = 110$ K, followed by a second transition to a commensurate CDW state around 80 K [9–11]. Although the structural observations seem to be uncontroversial, the corresponding effects on the electronic structure are ambiguous. Angle resolved photoemission spectroscopy (ARPES) studies report on a CDW induced gap around the $\overline{M}$-point of the Fermi surface only as a shift of a secondary peak, although a clear spectral intensity suppression at the Fermi level is absent [12–15]. Alternatively, a recent STM study observes a gap around the Γ-point [16] i.e. not compatible with the CDW nesting mechanism. Additionally, the expected CDW Fermi surface nesting along the k_z direction has been linked to a band warping effect [13, 14, 17], while this is still awaiting to be repeated above the CDW transition temperature (T^*).

The experimental results are even more elusive and contradictory in the monolayer VSe_2 samples. First, a fully gapped Fermi surface has been reported in multiple studies [18–20]. Such observation is unlikely for a CDW phase because the CDW wave vector would not be defined. Second, monolayer samples seem to have a larger gap (∼100 meV) and higher T^* while the experimental band structures do not exhibit any signature of backbending to support such a large energy gap in contrast to the computational models [18–20].

Here we re-examine the electronic structure of VSe_2 performing a series of dedicated ARPES experiments. While reproducing many of the earlier results, a closer examination reveals a surprisingly richer surface electronic structure than previously reported. In light of this more complete band structure, the presence of apparent gaps and warping effects are seen as resulting from the combined dispersion of closely laying multiple bands close to the Fermi level. Furthermore, the absence of localized gaps (both *in-* and *out-of-plane*) at the Fermi level rules out a CDW scenario as the likely origin of the observed structural phase transition in VSe_2.

II. EXPERIMENTAL AND COMPUTATIONAL METHODS

Single crystal 1T-VSe_2 were obtained from 2dsemiconductors company. ARPES experiments were performed at 21-ID-1 (ESM) beamline of NSLS-II using a DA30 Scienta electron spectrometer with an energy resolution better than 12 meV and a beam spot size of approximately 5 μm^2. The synchrotron radiation incidence angle was 55^o. Analyzer slit was along to the $\overline{M}$ - $\overline{\Gamma}$ - $\overline{M'}$ direction during the ARPES measurements at normal emission and along to the $\overline{K}$ - $\overline{K'}$-direction during the zone corner scans. In linear vertical (LV) polarized light the electric field is parallel to the sample surface and analyzer slit while in linear horizontal (LH) polarized light is on the incident plane. Band structure calculation is performed with Quantum Espresso package [21, 22]. The photon energy is converted to k_z crystal momentum assuming

* tyilmaz@bnl.gov

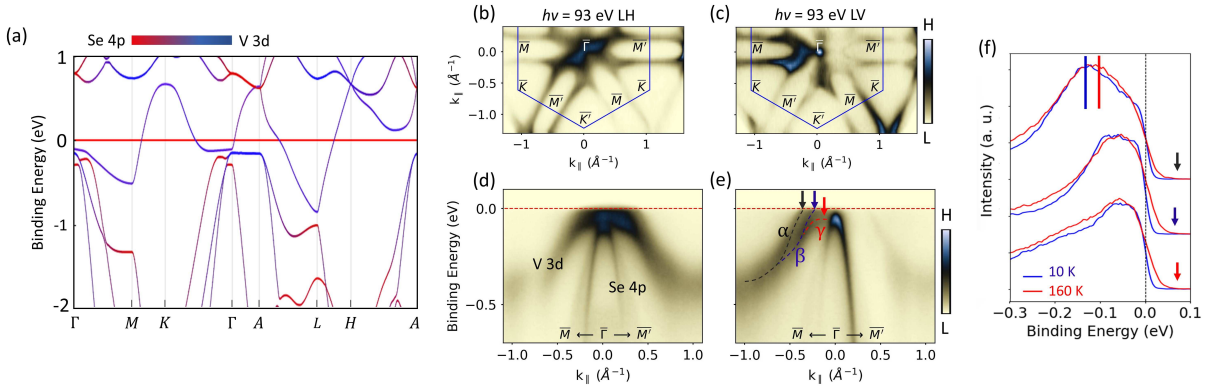

FIG. 1. (a) Orbital projected band structure of the bulk VSe_2 in normal state without spin-orbit coupling. The red horizontal line represents the Fermi level. (b-c) Fermi surfaces of a bulk 1T-VSe_2 sample taken at 10 K with 93 eV LH and LV polarized lights, respectively. (d-e) Corresponding ARPES maps along the $\overline{M}$- $\overline{\Gamma}$ - $\overline{M'}$ direction. The asymmetric band structure observed with LV polarized lights is likely due to the 3-fold rotational symmetry of the band structure. (f) EDCs taken along the black, blue, and red arrows shown in (e). To further support the existence of multiple bands, EDC analyses are given in Appendix A. ARPES data without guiding lines and the one with superimposed calculated band structure can also be found in Appendix A.

the free electron final state approximation given as $\hbar k_z = 2m_e\sqrt{E_{kin}\cos(\theta) + V_o}$ where m_e is the free electron mass, E_{kin} is the photoelectron kinetic energy, and V_o, inner potential, set to 7.5 eV [17].

III. EXPERIMENTAL RESULTS

The computed electronic structure of VSe_2 is presented in Figure 1(a) for comparison with the experimental one. The Fermi level is dominated by V 3d atomic orbitals which form V-shaped bulk bands at $M(L)$-point and exhibit relatively flatter features near the zone center. Highly dispersive Se 4p atomic orbitals are mostly located around the $\Gamma(A)$-point starting from just below the Fermi level. Furthermore, the V 3d atomic orbitals do not exhibit any splitting near the $\Gamma(A)$ or $M(L)$-point. Particularly, a single band is crossing the Fermi level in the vicinity of the $M(L)$-point. Although this band structure is in excellent agreement with previous studies [23, 24], it fails to reproduce all the experimental details as we will discuss below.

The experimental electronic structure of 1T-VSe_2 bulk samples examined with LH and LV polarized light is presented in Figure 1(b-e), respectively. In the LH geometry, ellipsoidal electron pockets centered at $\overline{M}(\overline{M'})$-point are the main features of the Fermi surface while highly dispersive Se 4p atomic orbitals dominate the zone center (Figure 1(b)). The corresponding ARPES map along the $\overline{M}$-$\overline{\Gamma}$-$\overline{M'}$ exhibits V-3d atomic orbitals with nearly flat dispersion in the vicinity of the $\overline{\Gamma}$-point where it overlaps with Se 4p atomic orbitals (Figure 1(d)). The band structure obtained in this particular experimental geometry is consistent with the computed one as well as with earlier ARPES reports [14, 17, 18, 23, 24].

On the other hand, the same band structure taken with LV polarized light reveals differences in details. The zone center exhibits a point like dispersion, enabling the study of the band structure around the $\overline{\Gamma}$-point more precisely. Unlike the single band observed with LH polarized light, three bands, named α, β, and γ, are now resolved around the zone center (Figure 1(e)). The first two bands are crossing the Fermi level at $k_{\parallel}$ = -0.37 $\mathring{A}^{-1}$ and at $k_{\parallel}$ = -0.24 $\mathring{A}^{-1}$ while the third band is located just below the Fermi level displaying a flatter dispersion towards the $\overline{\Gamma}$-point. These additional states are not predicted in the band structure calculation reported here or elsewhere [14, 17, 18, 23, 24]. The implication for the CDW induced gap is that if a band is located just below the Fermi level, temperature induced lifetime broadening can always lead to a determination of a false gap. This is likely to be the case in a recent STM study that reports a prominent gap in the vicinity of the $\overline{\Gamma}$-point [16]. Furthermore, these closely laying multiple bands are a major characteristic of the material and can be resolved at any temperature, regardless of T^*, showing that their origin is independent of the structural distortion (Appendix A).

By using this new finding, one can reproduce data that appear to host a temperature dependent gap at the Fermi level. The EDCs corresponding to the arrows in Figure 1(e) are given in Figure 1(f) for two temperatures; 10 K and 160 K (below and above T^*). Clearly, in all three cases there is no evidence of a CDW gap, the intensity at the Fermi level showing no prominent temperature dependence. However, the spectra further away from $\overline{\Gamma}$ displays a shift towards higher binding energy at low temperature (blue and red vertical lines in Figure 1(f)). Such shift is commonly attributed to a gap opening in this material [12, 13, 15], but it is more simply explained by temperature induced lifetime broadening of the bands with increased emission in the overlapping region between the α and β bands. Indeed, lack of resolving these bands in

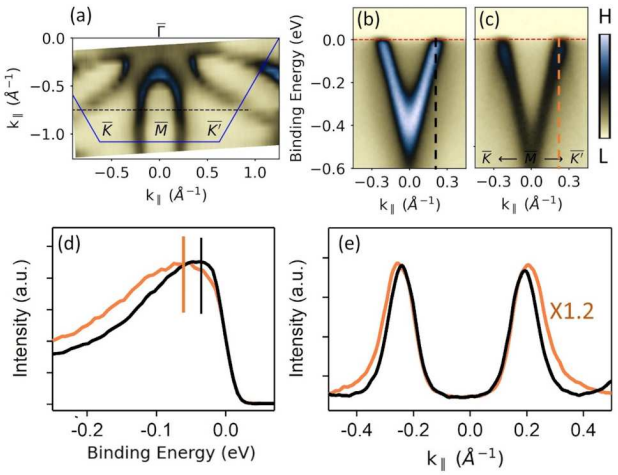

FIG. 2. (a) Fermi surface recorded at 93 eV with LH polarized light. (b-c) ARPES maps taken along the dashed black line in (a) and along the $\overline{K}$- $\overline{M}$ - $\overline{K'}$, respectively. (d) EDCs taken along the dashed black and orange lines in (b-c). Vertical black and orange lines in (d) mark the high intensity points. (e) MDCs taken at the Fermi level from (b-c).

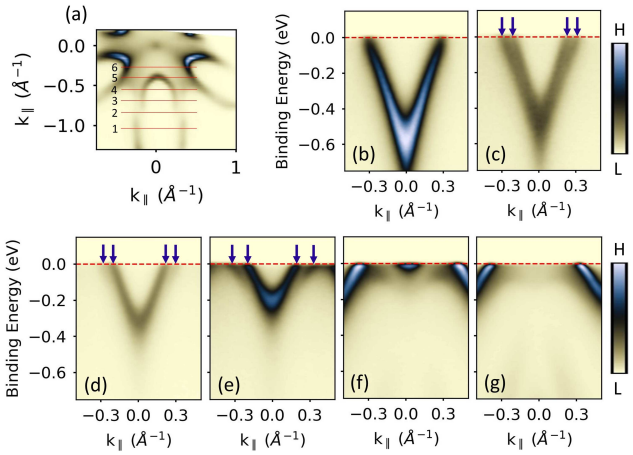

FIG. 3. (a) The Fermi surface. (b-g) ARPES cuts along the 1-6 lines shown in (a), respectively. Spectrum (b) is along the $\overline{K}$- $\overline{M}$ - $\overline{K'}$ high symmetry direction. Blue arrows mark the double bands. All spectra were collected at 75 eV with LH polarized light at 10 K.

the earlier studies led to misinterpreting the experimental data. Furthermore, temperature dependent EDCs from LV polarized light around the $\overline{M}(\overline{M'})$ are also displayed in Appendix A and confirm the absence of a gap at the Fermi level across the structural transition.

In other studies, the modulation of the color contrast on the electronic structure figures is relied on as a signature of a gap opening at the Fermi level [13, 14]. Here, we repeat a similar experiment. Figure 2(a) presents the Fermi surface that covers the ellipsoidal electron pocket centered at the $\overline{M}$-point. Color-contrast is gradually decreasing towards $\overline{M}$-point, consistently with the earlier studies. In this regard, one can claim a possible gap opening at the Brillouin zone boundaries. To check if this is the case, a logical experimental approach will be comparing the Fermi edges taken from the different portions of the Fermi surface recorded below T*. In this way, possible experimental errors induced by variable temperature can be avoided. The ARPES maps taken along the dashed black line and along the $\overline{K}$ - $\overline{M}$ - $\overline{K'}$ direction are given in Figure 2(b-c), respectively. Compared to the former one, the latter exhibits lower spectral intensity in the entire band structure rather than only at the Fermi level. Therefore, the apparent spectral intensity does not necessarily represent a gap opening. Indeed, the EDCs taken along the dashed black and orange lines (Figure 2(d)) exhibit the same Fermi level indicating the absence of an insulating gap. On the other hand, the high intensity points show a difference in the EDCs (vertical orange and black lines in Figure 2(d)). This apparent shift has been considered as a well-established experimental signature of the CDW induced gap in VSe_2 [12–15] but could be explained by the existence of closely laying multiple bands.

To further pursue this hypothesis, the MDCs taken at the Fermi level of Figure 2(b-c) are compared in Figure 2(e). The one along the $\overline{K}$ - $\overline{M}$ - $\overline{K'}$ direction exhibits not only a lower intensity but also a broader line shape compared to the other one. Therefore, the lower intensity around $\overline{M}$ of the Fermi surface is not due to a gap opening but it is caused by a broader electronic structure in momentum space, indicating the presence of multiple band dispersion.

The band structure is indeed more complex and involves closely laying multiple bands forming the ellipsoidal Fermi surface centered at $\overline{M}$ is experimentally confirmed by following the various ARPES maps parallel to $\overline{K}$ - $\overline{M}$ - $\overline{K'}$. For example at 75 eV photon energy, around the $\overline{M}$-point a single V-shape band appears crossing the Fermi level at $k_{\parallel} = \pm\ 0.32\ \AA$ (Figure 3(b)). However, this band splits towards the zone center (see blue arrow in Figure 3(c-e)). These additional bands eventually connect with the neighbor electron pockets. We also found that the LV polarized light is a powerful tool to probe these closely laying multiple bands in more detail as given in Appendix A. Depending on the photon energies, the multi band crossing at the Fermi level can be well resolved.

Closely laying multiple bands can be also probed in the band structure along the $\overline{K}$ - $\overline{M}$ - $\overline{K'}$ with a more elaborate approach. Fermi surfaces taken at various photon energies are given in Figure 4(a). In the data, 80 eV and 97 eV photons correspond to $k_z = A$ and $k_z = \Gamma$ high symmetry points in 2D momentum plane. The ellipsoidal pocket centered at $\overline{M}$-point shows a strong photon energy dependence, evolving to a dog-bone shape at $k_z = \Gamma$. In addition to this strong spectral feature, the second band with a weaker intensity is also visually observed in some

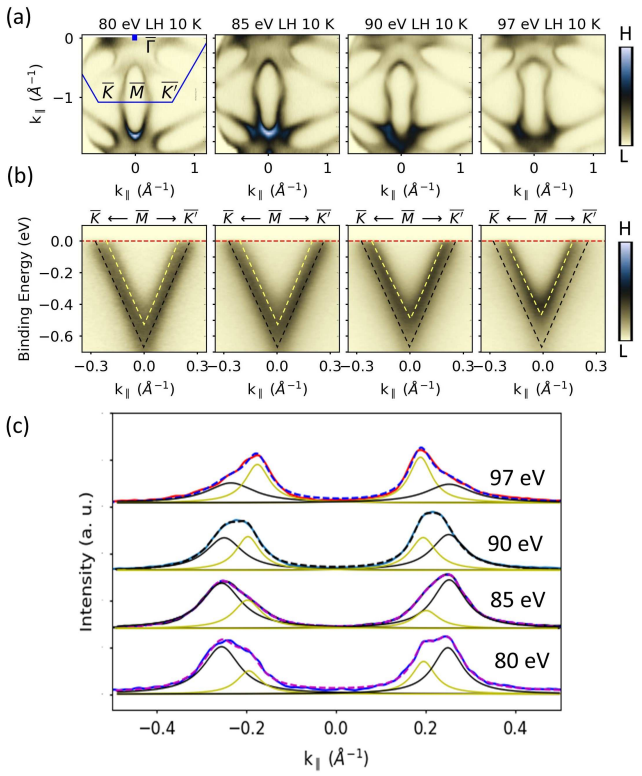

FIG. 4. (a-b) The Fermi surfaces and corresponding ARPES maps along $\overline{K}$- $\overline{M}$ - $\overline{K'}$ direction. (c) MDCs taken at the Fermi level from each spectrum in (b). Yellow and black lines in (c) are the Lorentzian components resulting from the fittings and the dashed lines are the sums.

parts of the Fermi surface. These closely laying multiple bands can be seen in ARPES maps along $\overline{K}$ - $\overline{M}$ - $\overline{K}'$ as marked with dashed yellow and black lines (Figure 4(b)).

To further support this observation, the MDCs taken at the Fermi level are compared in Figure 4(c). Bands located at $\pm$ $k_{\|}$ with respect to $\overline{M}$-point exhibit double peak features as indicated with yellow and black fitting lines. Thereby, the V-shape conduction band is indeed formed by two bands; inner and outer ones. Based on Figure 4(b-c), these two bands have distinct k_z dispersion as the outer band is 2D like while the inner one has 3D character and their spectral intensities show an opposite k_z dependence. This has an important implication for the CDW phase of the VSe_2. One of the fundamental experimental evidence for the CDW phase was reported to be a warping effect on the Fermi surface along the k_z direction [13, 14, 17]. However, this warping effect is clearly due to the different nature of these closely laying multiple bands crossing the Fermi level and is not correlated with any type of structural distortion. Indeed, the apparent warping of the band structure is temperature independent (Appendix A). Therefore, earlier observations, failing to resolve these closely laying multiple bands, lead to misinterpretation of the experimental data.

Our observations also suggest that the large CDW induced gap of around 100 meV in the monolayer VSe_2 is questionable [18–20]. This is discussed in Appendix B and no gap is detected around the $\overline{M}$-point that can be associated with the CDW phase. Furthermore, the apparent width of the Fermi edge around the $\overline{M}$-point does not change with the temperature in the monolayer case. This indicates that it is dominated by temperature independent defects such as vacancies.

IV. CONCLUSION

In summary, we show that the Fermi surface of VSe_2 is dominated by closely laying multiple bands. Using this evidence and the absence of any Fermi gap, each of the previous observations can be explained and shown to be unrelated to the structural transition of VSe_2. Based on the data given in Figure 4, a two-dimensional surface state could be the origin of closely laying multiple bands. However, considering that transport measurements consistently show an anomaly around 110 K [25–27], a modification on the band structure is expected across the same temperature. An alternative to the gap-opening/CDW scenario could be a change of the Fermi surface area. Such transition would be somewhat similar to the nematic transitions commonly observed in the Fe-based superconductors. However, this requires further detailed studies concentrating on this particular point since the multiple bands located at the Fermi level complicates the experiments. Nevertheless, the present work, providing a more complete band structure of 1T-VSe_2, should constitute a solid base to study the true nature of the structural distortion in this material. Therefore, it is expected that present results should pave the way for future works on the topic.

ACKNOWLEDGMENTS

This research used resources ESM (21ID-I) beamline of the National Synchrotron Light Source II, a U.S. Department of Energy (DOE) Office of Science User Facility operated for the DOE Office of Science by Brookhaven National Laboratory under Contract No. DE-SC0012704. We have no conflict of interest, financial or other to declare.

Appendix A: Electronic structure of the bulk VSe_2

This section provides further details of the band structure in bulk VSe_2 to support the observations in the main text. Photon energy and temperature dependent electronic structure of the bulk sample are outlined to demonstrate the independence of the multiple bands from the CDW order.

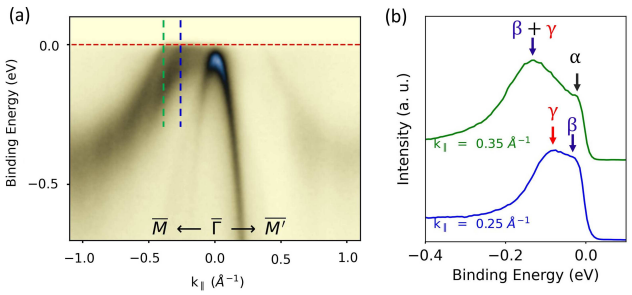

FIG. 5. (a) ARPES data taken at 10 K with 93 eV LV polarized light along the $\overline{M}$ - $\overline{\Gamma}$ - $\overline{M'}$ direction. (b) Integrated EDCs along the dashed green and blue lines within $\delta k_\parallel = 0.11$ $\AA^{-1}$. Corresponding momentum points are given under each spectrum. The α, β, and γ bands are marked with arrows.

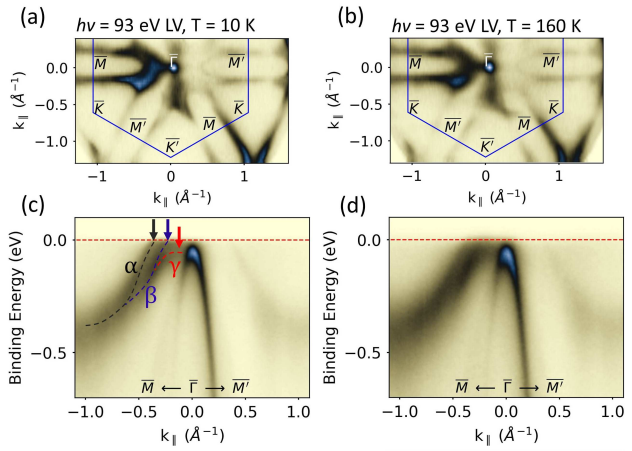

FIG. 6. (a-b) Fermi surfaces taken at 10 K and 160 K, respectively. (c-d) Corresponding ARPES maps along the $\overline{M}$ - $\overline{\Gamma}$ - $\overline{M'}$ direction. The data is obtained with 93 eV LV polarized light.

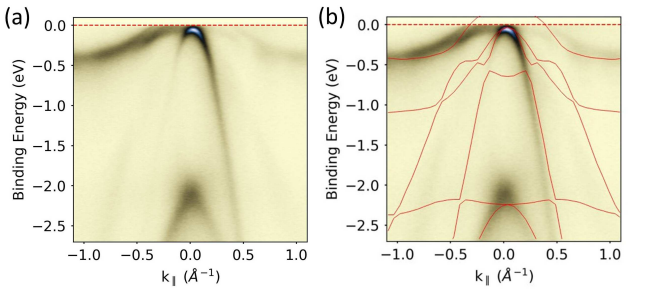

FIG. 7. (a) Raw ARPES data taken with 93 eV LV light along the $\overline{M}$ - $\overline{\Gamma}$ - $\overline{M'}$ direction. (b) Same data with the superimposed calculated band structure. Data are measured at 10 K. Se bands in the zone center are taken as reference and the calculated band structure is 0.12 eV shifted up.

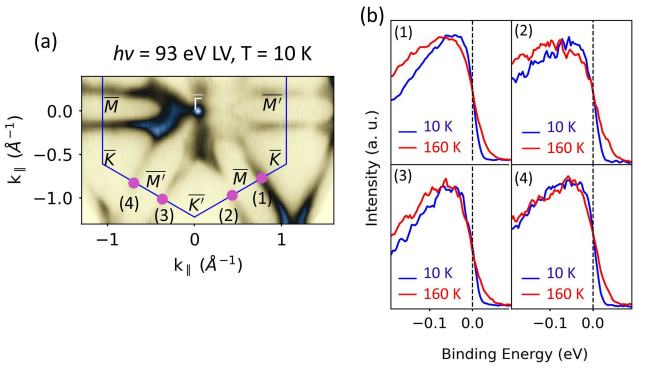

FIG. 8. (a) Fermi surface taken at 10 K with 93 eV LV polarized light. (b) Temperature dependent EDCs taken at the k-points marked in (a) with numbered pink points.

First, the EDCs taken at different $k_\parallel$-points are compared to show how multiple peaks can be observed in the vicinity of the Fermi level. As shown in Figure 5(a), the α and β bands cross the Fermi level while the γ band locates below the Fermi level with a relatively flat dispersion in the vicinity of the $\overline{\Gamma}$-point. The spectral peaks stemming from each band can be seen in the EDCs given in Figure 5(b). Due to their different binding energies for the same $k_\parallel$, an apparent gap can be claimed as an observation of the secondary peak. On the other hand, the system is metallic without an energy gap at the Fermi level. Furthermore, The α, β, and γ bands can be resolved above and below the T^* of 110 K (Figure 6). This confirms that these multiple bands are independent of the structural distortion.

In order to directly compare the theoretical and raw experimental band structure, Raw ARPES data and superimposed calculated band structure are given in Figure 7(a-b), respectively. Despite the overall agreement, a clear mismatch between theory and experiment is found for the V 3d band in the vicinity of the Fermi level. Theory shows a single branch crossing the Fermi level. On the other hand, experimental band structure displays multiple bands, and the γ is located below the Fermi level (Figure 7(b)).

An energy gap at the Fermi level is further investigated by taking various EDCs at the different points of the Fermi surface as marked in Figure 8(a) and comparing them for the temperatures below and above the T^*. All the EDCs taken at 10 K and 160 K exhibits the same Fermi level showing the absence of a gap opening due to the CDW order.

By using the LV polarized lights, multiple bands crossing the Fermi level can be probed as shown in Figure 9. Their spectral intensity dramatically varies as a function of the photon energy. This is likely to be the main origin of the false k_z dependent Fermi gap reported in the previous studies

In previous studies, the warping of bands along the k_z direction was attributed to CDW induced nesting [13, 14, 17]. However, up to date, this claim has not been investigated as a function of the temperature. The warping effect, however, can be observed below and above the T^* as shown in Figure 10. Hence, it cannot be associated

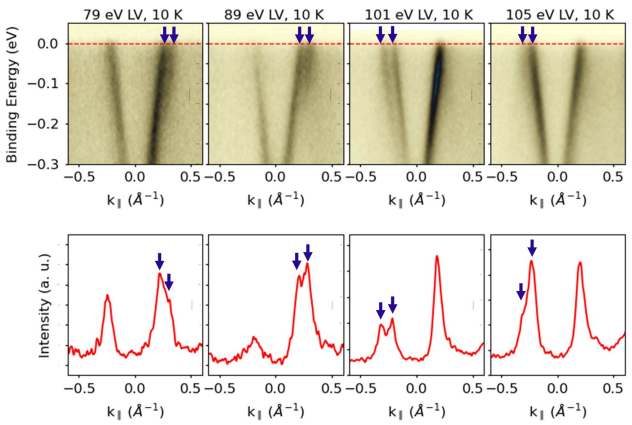

FIG. 9. (a) Photon energy dependent ARPES maps taken with LV polarized lights along the $\overline{M}$ - $\overline{M'}$ direction. (b) Corresponding MDC cuts at the Fermi level. Blue arrows mark the multiple bands.

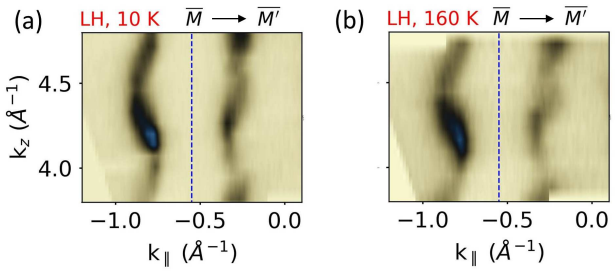

FIG. 10. (a-b) Photon energy dependent band structure at 10 K and 160 K, respectively.

with the CDW phase.

Appendix B: Electronic structure of the monolayer VSe_2

ARPES maps recorded at 10 K and 250 K from a monolayer VSe_2 sample are given in Figure 11(a-b), respectively. As consistent with previous observations, there appears to be a suppression of a spectral intensity at the Fermi level but this seems to exist at both temperatures. In the previous studies, the CDW induced gap is emphasized in symmetrized EDCs [18–20]. Here we follow the evolution of the Fermi edge as a function of temperature. This is essential since the CDW induced gap is a pseudogap. The temperature dependent EDCs taken along the dashed black line in Figure 11(a) are given in Figure 11(c) and 11(d). Clearly, the EDCs do not exhibit any gap when directly compared to each other and with the Fermi level of an Au reference. More importantly, the width of the Fermi edge does not change with the temperature, indicating the dominant role of defects, such as Se-vacancies. It is therefore unlikely for a CDW phase to survive in the monolayer sample. Although the STM studies show the formations of a periodic lattice superstructure below T*, it could be local or represent a trivial structural transition.

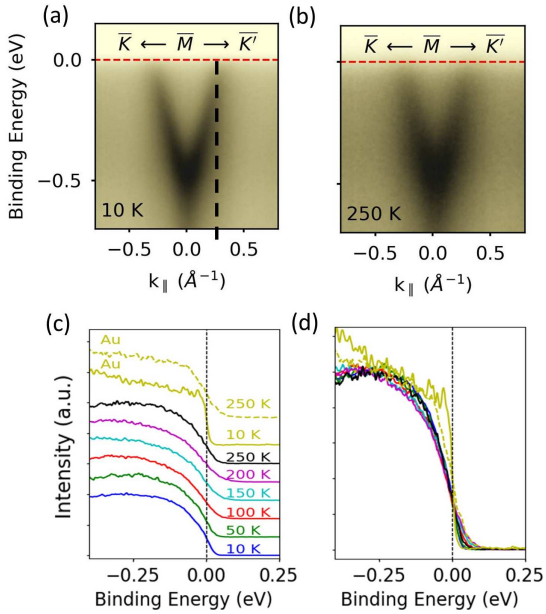

FIG. 11. (a-b) ARPES maps taken along the $\overline{K}$ - $\overline{M}$ - $\overline{K'}$ direction at 10 K and 250 K, respectively from a monolayer VSe_2. (c) Temperature dependent EDCs taken along the black dashed line shown (a). (d) Same EDCs but superimposed. Data were collected with 93 eV LH polarized light from a sample grown on a HOPG substrate at 543 K with molecular beam epitaxy.

Furthermore, multiple studies reported a fully gaped Fermi surface with a size as large as 100 meV [18–20]. Such a large gap is expected to induce a visible backbending at the Fermi level which is the main mechanism behind the gap opening in the CDW phase. However, neither of the previous reports shows such spectral anomaly within the same studies. Observation of a gap on the entire Fermi surface is also elusive since the CDW wave vector would have no influence in that a case.

[1] K. F. Mak and J. Shan, Photonics and optoelectronics of 2d semiconductor transition metal dichalcogenides, Nature Photonics **10**, 216 (2016).

[2] S. Manzeli, D. Ovchinnikov, D. Pasquier, O. V. Yazyev, and A. Kis, 2d transition metal dichalcogenides, Nature Reviews Materials **2**, 1 (2017).

[3] K. Cho, M. Kończykowski, S. Teknowijoyo, M. A. Tanatar, J. Guss, P. Gartin, J. Wilde, A. Kreyssig, R. McQueeney, A. I. Goldman, *et al.*, Using controlled disorder to probe the interplay between charge order and superconductivity in nbse2, Nature communications **9**, 1 (2018).

[4] F. Yu, D. Ma, W. Zhuo, S. Liu, X. Wen, B. Lei, J. Ying, and X. Chen, Unusual competition of superconductivity and charge-density-wave state in a compressed topological kagome metal, Nature communications **12**, 1 (2021).

[5] G. Grüner, The dynamics of charge-density waves, Reviews of modern physics **60**, 1129 (1988).

[6] P. Monceau, Electronic crystals: an experimental overview, Advances in Physics **61**, 325 (2012).

[7] J. Wilson, F. Di Salvo, and S. Mahajan, Charge-density waves in metallic, layered, transition-metal dichalcogenides, Physical review letters **32**, 882 (1974).

[8] C. Wang, C. Slough, and R. Coleman, Spectroscopy of dichalcogenides and trichalcogenides using scanning tunneling microscopy, Journal of Vacuum Science & Technology B: Microelectronics and Nanometer Structures Processing, Measurement, and Phenomena **9**, 1048 (1991).

[9] B. Giambattista, C. G. Slough, W. W. McNairy, and R. V. Coleman, Scanning tunneling microscopy of atoms and charge-density waves in 1t-tas 2, 1t-tase 2, and 1t-vse 2, Physical Review B **41**, 10082 (1990).

[10] D. Eaglesham, R. Withers, and D. Bird, Charge-density-wave transitions in 1t-vse2, Journal of Physics C: Solid State Physics **19**, 359 (1986).

[11] K. Tsutsumi, X-ray-diffraction study of the periodic lattice distortion associated with a charge-density wave in 1 t-v se 2, Physical Review B **26**, 5756 (1982).

[12] K. Terashima, T. Sato, H. Komatsu, T. Takahashi, N. Maeda, and K. Hayashi, Charge-density wave transition of 1 t- v s e 2 studied by angle-resolved photoemission spectroscopy, Physical Review B **68**, 155108 (2003).

[13] T. Sato, K. Terashima, S. Souma, H. Matsui, T. Takahashi, H. Yang, S. Wang, H. Ding, N. Maeda, and K. Hayashi, Three-dimensional fermi-surface nesting in 1t-vse2 studied by angle-resolved photoemission spectroscopy, journal of the physical society of japan **73**, 3331 (2004).

[14] Z. Wang, Q. Yin, S. Yan, L. Wu, X. Wu, M. Li, W. Song, Q. Liu, H. Ma, W. Ji, *et al.*, Three-dimensional charge density wave observed by angle-resolved photoemission spectroscopy in 1 t- vse 2, Physical Review B **104**, 155134 (2021).

[15] Y. Falke, N. Ehlen, G. Marini, A. V. Fedorov, V. Y. Voroshnin, B. V. Senkovskiy, K. Nikonov, M. Hoesch, T. K. Kim, L. Petaccia, *et al.*, Coupling to zone-center optical phonons in v se 2 enhanced by charge density waves, Physical Review B **104**, 235137 (2021).

[16] W. Jolie, T. Knispel, N. Ehlen, K. Nikonov, C. Busse, A. Gruneis, and T. Michely, Charge density wave phase of vse 2 revisited, Physical Review B **99**, 115417 (2019).

[17] V. N. Strocov, M. Shi, M. Kobayashi, C. Monney, X. Wang, J. Krempasky, T. Schmitt, L. Patthey, H. Berger, and P. Blaha, Three-dimensional electron realm in vse 2 by soft-x-ray photoelectron spectroscopy: Origin of charge-density waves, Physical Review Letters **109**, 086401 (2012).

[18] P. Chen, W. W. Pai, Y.-H. Chan, V. Madhavan, M.-Y. Chou, S.-K. Mo, A.-V. Fedorov, and T.-C. Chiang, Unique gap structure and symmetry of the charge density wave in single-layer vse 2, Physical review letters **121**, 196402 (2018).

[19] J. Feng, D. Biswas, A. Rajan, M. D. Watson, F. Mazzola, O. J. Clark, K. Underwood, I. Markovic, M. McLaren, A. Hunter, *et al.*, Electronic structure and enhanced charge-density wave order of monolayer vse2, Nano letters **18**, 4493 (2018).

[20] J. Zong, Y. Xie, Q. Meng, Q. Tian, W. Chen, X. Xie, S. Jin, Y. Zhang, L. Wang, W. Ren, *et al.*, Observation of multiple charge density wave phases in epitaxial monolayer 1t-vse2 film, Chinese Physics B **31**, 107301 (2022).

[21] P. Giannozzi, S. Baroni, N. Bonini, M. Calandra, R. Car, C. Cavazzoni, D. Ceresoli, G. L. Chiarotti, M. Cococcioni, I. Dabo, *et al.*, Quantum espresso: a modular and open-source software project for quantum simulations of materials, Journal of physics: Condensed matter **21**, 395502 (2009).

[22] P. Giannozzi, O. Andreussi, T. Brumme, O. Bunau, M. B. Nardelli, M. Calandra, R. Car, C. Cavazzoni, D. Ceresoli, M. Cococcioni, *et al.*, Advanced capabilities for materials modelling with quantum espresso, Journal of physics: Condensed matter **29**, 465901 (2017).

[23] J. He, Q. Xie, and G. Xu, Confinement effect enhanced stoner ferromagnetic instability in monolayer 1t-vse2, New Journal of Physics **23**, 023027 (2021).

[24] P. M. Coelho, K. Nguyen Cong, M. Bonilla, S. Kolekar, M.-H. Phan, J. Avila, M. C. Asensio, I. I. Oleynik, and M. Batzill, Charge density wave state suppresses ferromagnetic ordering in vse2 monolayers, The Journal of Physical Chemistry C **123**, 14089 (2019).

[25] A. H. Thompson and B. G. Silbernagel, Correlated magnetic and transport properties in the charge-density-wave states of v se 2, Physical Review B **19**, 3420 (1979).

[26] D. Li, X. Wang, C.-m. Kan, D. He, Z. Li, Q. Hao, H. Zhao, C. Wu, C. Jin, and X. Cui, Structural phase transition of multilayer vse2, ACS applied materials & interfaces **12**, 25143 (2020).

[27] D. Song, Y. Zhou, M. Zhang, X. He, and X. Li, Structural and transport properties of 1 t-vse2 single crystal under high pressures, Frontiers in Materials **8**, 710849 (2021).